

Structural Arrest in an Ideal Gas

Willem van Ketel,^{1,2} Chinmay Das,^{1,3} and Daan Frenkel¹

¹*FOM Institute for Atomic and Molecular Physics, Kruislaan 407, 1098 SJ Amsterdam, The Netherlands*

²*Willem de Zwijgercollege, Nieuwe 's Gravelandseweg 38, 1405 HM Bussum, The Netherlands*

³*Department of Applied Mathematics, University of Leeds, Leeds LS2 9JT, United Kingdom*

(Received 3 November 2004; published 8 April 2005)

We report a molecular dynamics study of a simple model system that has the static properties of an ideal gas, yet exhibits nontrivial “glassy” dynamics behavior at high densities. The constituent molecules of this system are constructs of three infinitely thin hard rods of length L , rigidly joined at their midpoints. The crosses have random but fixed orientation. The static properties of this system are those of an ideal gas, and its collision frequency can be computed analytically. For number densities $NL^3/V \gg 1$, the single-particle diffusivity goes to zero. As the system is completely structureless, standard mode-coupling theory cannot describe the observed structural arrest. Nevertheless, the system exhibits many dynamical features that appear to be mode-coupling-like. All high-density incoherent intermediate scattering functions collapse onto master curves that depend only on the wave vector.

DOI: 10.1103/PhysRevLett.94.135703

PACS numbers: 64.70.Pf, 05.10.-a, 07.05.Tp

There probably exist more theories for the glass transition than for any other phenomenon in condensed matter physics except high- T_c superconductivity (see, e.g., [1–7]). Some of these theories assume that the glass transition reflects an underlying (possibly frustrated) thermodynamic phase transition, others describe the glass transition as a purely kinetic phenomenon. One of the most widely used theories of the glass transition is mode-coupling theory (MCT) [3,4,8]. In the standard version of MCT, the glass transition is kinetic in nature but it is caused by the existence of static structural correlations in the system that vitrifies. It is probably fruitless to search for the “true” theory of the glass transition, because not all glasses appear to be equivalent [9,10]. However, it is important to disentangle, as much as possible, the roles of structural correlations and purely kinetic effects in the absence of such correlations. In the present Letter, we report simulations of a model system that has the structural properties of an ideal gas. If this system undergoes dynamical arrest, this is a purely kinetic effect. Our aim is to describe the characteristic features of vitrification in this ideal gas.

The model system that we use contains particles that consist of three mutually perpendicular line segments of length L , rigidly joined at their midpoints. This system of 3D “crosses” is a generalization of the hard-needle model that had been developed to study topological effects on rotational and translational diffusion [11]. Earlier papers already implicitly [2] or explicitly [12] suggested that systems consisting of rigidly joined line segments might provide interesting models to study the glass transition. However, to our knowledge, no numerical studies of such ideal 3D glass formers have been reported. Rather, a lattice-based version of the hard-needle model has been studied by several authors as a model for orientational glass formers [13]. In general, crosses have both translational and rotational motion. However, as we focus on the

normal (translational) glass transition, we suppress the rotational motion of the crosses (infinite moment of inertia). This greatly speeds up the simulations. We expect that the suppression of rotational motion does not qualitatively affect the translational structural arrest. Of course, this remains to be demonstrated. As the crosses have zero volume and zero excluded volume, *all* static thermodynamic quantities are exactly known. By random insertion, one can trivially generate a representative equilibrium configuration at any density. As our model is an ideal gas, it has no thermodynamic phase transitions. However, as we discuss below, the dynamics are highly nontrivial. In our simulations, we choose the length L of the arms of the cross as the unit of length, the thermal energy, $k_B T$ as the unit of energy, and the mass m of a particle as the unit of mass. Initial configurations were generated by inserting particles with random position and orientation into the simulation box. The particles were given a Maxwellian velocity distribution. The total momentum was set equal to zero. We employed simple cubic periodic boundary conditions. We use an event-based molecular dynamics simulation to study the dynamics similar to the method described in Ref. [14]. During a collision, the momentum components perpendicular to the plane containing the two colliding arms are exchanged. Most runs were performed on systems of 512, 1728, and 4096 particles. We found that finite-size effects were negligible in the density regime that we studied. The reduced densities [$\rho \equiv (NL^3/V)$] in our simulations varied from 1 to 27. As a test of the molecular dynamics algorithm, we computed the collision frequency Γ_c for all densities between $\rho = 1$ and 27 and compared it with the (exact) kinetic-theory expression $\Gamma_c = (9/4) \times \sqrt{\pi} \rho$. At all densities, the simulation data agree to within the statistical error with the analytical expression, suggesting that our algorithm does not miss collisions. In a typical run, results were obtained by averaging over ten indepen-

dent starting configurations. In addition, we averaged over 15 time origins separated by 5 time units. The simulations ran for the time it takes the smallest nonzero wave vector component of the dynamic structure factor $S(q, t)$ to decay to $1/e$, or for 10^9 collisions (whichever time is smaller). All components of $S(q, t)$ decay completely in 10^9 collisions for the 512- and 1728-particle systems.

After a ballistic regime ($\langle r^2 \rangle \sim t^2$), the mean-square displacement (MSD) becomes diffusive ($\langle r^2 \rangle \sim t$) at longer times (Fig. 1). The time interval between the ballistic and the diffusive regions increase with ρ . The long-time tagged-particle diffusivity (inset of Fig. 1) appears to decrease exponentially with increasing ρ . This suggests that the rate-limiting step in diffusion is the creation of a “cavity” around a particle, such that the topological constraints that inhibit its motion are relieved. The reversible work needed to create a volume ΔV is equal to $P\Delta V$. For an ideal gas ($P = \rho kT$) the probability to form a volume ΔV by a spontaneous fluctuation is $\exp(-\rho\Delta V)$. From the observed exponential density dependence of the diffusivity, we estimate that a cavity with volume $\Delta V^* \approx 0.45L^3$ is needed to enable diffusion. This exponential behavior of the diffusivity is very different from the algebraic density dependence of the rotational diffusion constant observed in systems of translationally fixed needles [13].

To gain a better understanding of the mechanism responsible for single-particle diffusion, we considered the probability distribution of the particle displacements at a fixed time interval. Both in the ballistic and diffusive regimes, the probability is Gaussian, but in between there are marked deviations from Gaussian behavior. $\alpha_2 \equiv \frac{3\langle r^4 \rangle}{5[\langle r^2 \rangle]^2} - 1$ gives a convenient measure of departure from Gaussian behavior [Fig. 2(a)]. Both the time range where

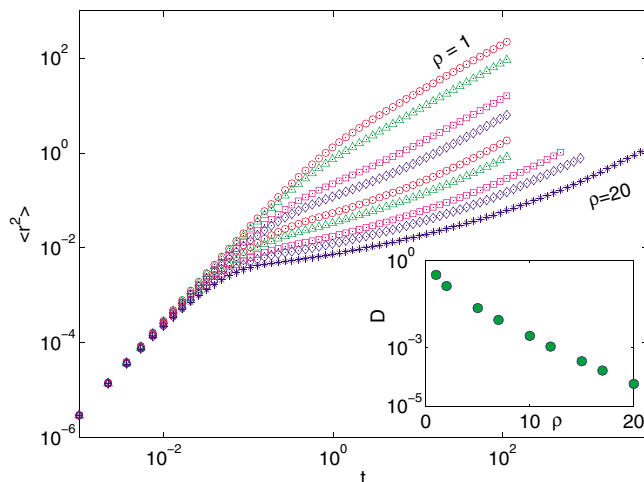


FIG. 1 (color online). Mean-square displacement of 3D crosses for different densities. For $t \leq \tau_{\text{col}}$, the motion is ballistic and $\langle r^2 \rangle \sim t^2$. At long times, the motion becomes diffusive ($\langle r^2 \rangle \sim t$). Inset: Tagged-particle diffusivity computed from the long-time behavior of the mean-squared displacement.

α_2 is significantly different from zero and the maximum magnitude of α_2 increase with ρ . One mechanism that can cause a non-Gaussian displacement distribution is the existence of inhomogeneities in the particle displacements [15]. In Fig. 2(b) we plot the percentage of the MSD carried by the 5% of the particles that have the largest displacement in the time interval considered (in what follows, we call these the “mobile particles”). The correlation of the fraction of the MSD carried by the most mobile particles with α_2 suggests that dynamic heterogeneity is the cause of non-Gaussian behavior in the present system. The long-time decay of the incoherent intermediate scattering function $F_s(q, t) \equiv \langle \frac{1}{N} \sum_j \exp\{i\vec{q} \cdot [\vec{r}_j(t) - \vec{r}_j(0)]\} \rangle$ appears to be slower than exponential at high densities (Fig. 5). The decay appears stretched exponential ($F_s(q, t) \approx \exp[-(t/\tau)^\beta]$), as is observed in many experiments on glassy systems. Such behavior is reproduced both in the mode-coupling picture [3] and in the (fundamentally different) dynamic facilitation theory [7]. The slope β is 2 for ballistic decay and 1 for diffusive decay (Fig. 3). For large ρ , β appears significantly smaller than 1.0 over a wide time interval and, as is shown in the inset of Fig. 3, a stretched exponential fits the long-time decay over almost three decades. However, a closer look shows that a stretched exponential cannot describe $F_s(q, t)$. This can be seen in Fig. 4, where we plot the time-dependent exponent of a local fit of $F_s(q, t)$ to a stretched exponential. The exponent β in Fig. 4 never reaches an intermediate plateau value. Rather, it varies with time and approaches the value $\beta = 1$ at long times. Hence, the long-time decay of $F_s(q, t)$ is simply exponential and it is nowhere stretched exponential. Several theories of the glass transition [16] give an

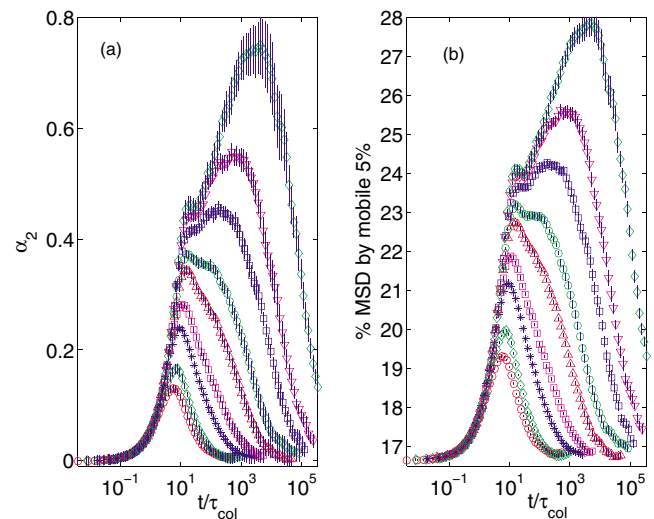


FIG. 2 (color online). Time dependence of (a) the non-Gaussian parameter α_2 and (b) the percentage of the MSD carried by the most mobile 5% particles. The maximum values of both function increase with increasing density. Densities: $\rho = 1, 2, 5, 7, 10, 12, 15, 17$, and 20.

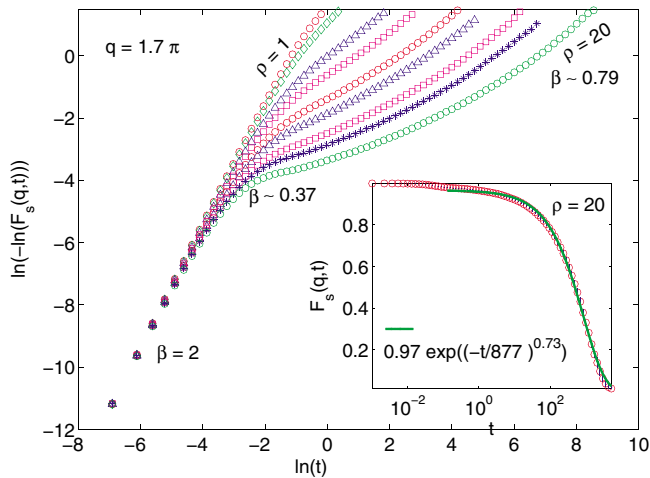


FIG. 3 (color online). Apparent stretched-exponential behavior of the intermediate scattering function. For $\rho = 20$, one can fit a stretched exponential $\exp[-(t/\tau)^\beta]$, with $\beta \approx 0.73$ to the non-ballistic decay of $F_s(q, t)$ (see inset). However, the apparent quality of the fit is misleading. A more careful analysis shows that no single stretched-exponential function fits the observed decay. As an illustration, a few local estimates of the exponent β are indicated in the figure.

explicit prediction for the time dependence of the stretching exponent β very similar to Fig. 4. Unfortunately, the theoretical results are rarely presented in this way. Yet, even though β itself is not well defined, it is still possible to study the dependence of the effective stretching exponent

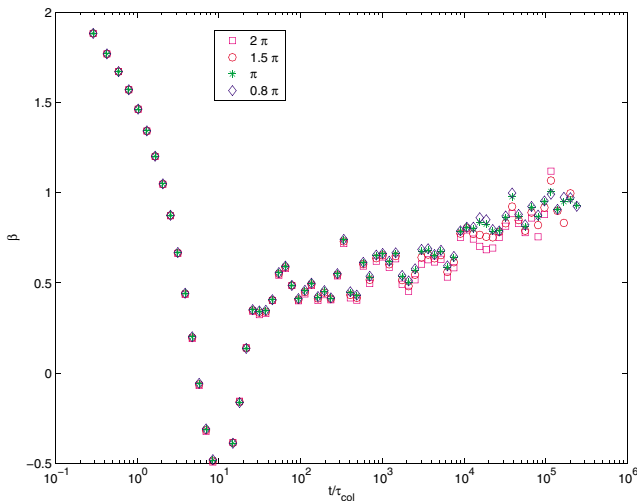


FIG. 4 (color online). The exponent of a local stretched-exponential fit for intermediate scattering function (see text). The description of $F_s(q, t)$ by a stretched exponential would only be meaningful if β would be constant over at least one decade in time. This is not the case. The data shown in the figure were obtained at a reduced density $\rho = 20$ and q vectors between 0.8π and 2π (in units L^{-1}). Similar plots at other densities show the same trend.

on density and wave vector. In our simulations, we find that, at fixed real (i.e., unscaled) time, β_{eff} appears independent of the wave vector q , but it does depend on the density.

The behavior of $F_s(q, t)$ at shorter times is also interesting. By plotting $F_s(q, t)$ as a function of t/τ_α , we can collapse the long-time behavior at all densities onto a single master curve (see Fig. 5). We define τ_α as the time at which $F_s(q, t) = 1/e$. For the highest densities ($\rho = 22$ and 27), the small- q components of $F_s(q, t)$ do not decay to $1/e$ within the simulation time. In that case, we estimate τ_α by optimizing the collapse on the master curve. We stress that this time-density scaling [17] of $F_s(q, t)$ is highly nontrivial. Götze has argued that it is one of the outstanding characteristics of MCT [3]. Yet, in the present case, standard MCT cannot apply. In Fig. 5 the collapse onto the master curve occurs sooner at higher densities. Note that this master curve has no short-time plateau. The absence of a short-time plateau is not surprising, as the ballistic regime ends when a particle hits the wall of its confining cage. The higher the density, the earlier the ballistic regime ends. Using the fact that the cage radius scales as $1/\rho$, we expect the master curve to behave at short times as $\exp\{-c/[\ln^2(t/\tau_\alpha)]\}$, which approaches smoothly to 1 as $t/\tau_\alpha \rightarrow 0$. This is indeed the behavior found (see inset of Fig. 5). On the time scales where non-Gaussian effects are most pronounced, a small fraction of the particles are responsible for most of the MSD. Figure 6 shows a typical snapshot of the 5% particles that were most mobile in a

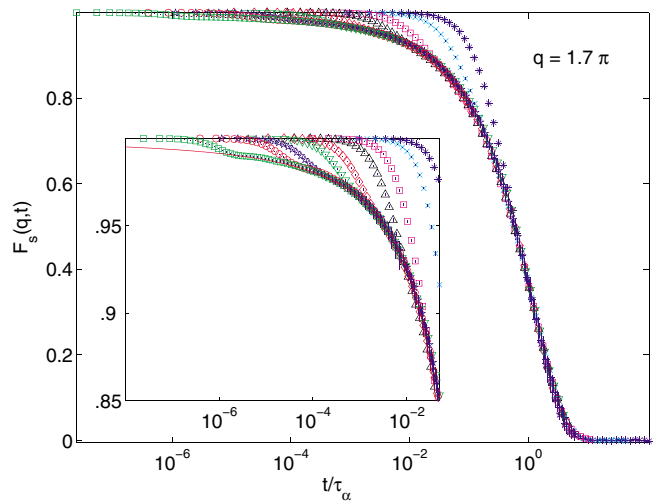


FIG. 5 (color online). Intermediate scattering function as a function of t/τ_α , where τ_α is the time constants of the long-time (“ α ”) decay of $F_s(q, t)$. The figure shows that, with increasing density, the $F_s(q, t)$ tend to collapse onto a single master curve. This master curve exhibits no plateau and decays exponentially for $t/\tau_\alpha \gg 1$. Inset: Short-time decay of $F_s(q, t)$ including a fit to the functional form $F_s(q, t) = \exp\{-c/[\ln^2(t/\tau_\alpha)]\}$, with $c \approx 1.647$. Simulations at densities $\rho = 5, 7, 10, 12, 15, 17, 20, 22$, and 27 .

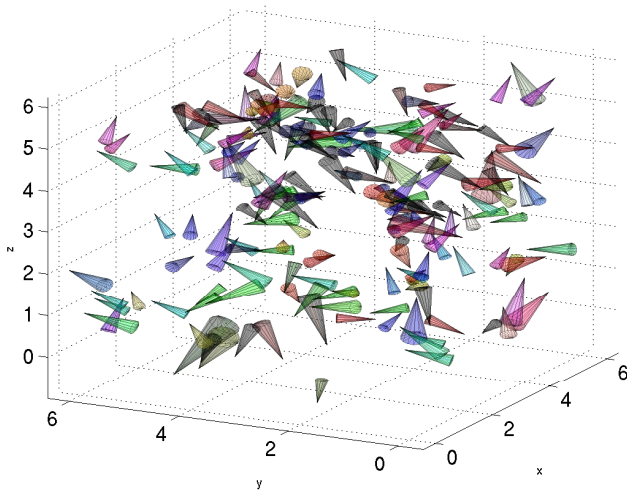


FIG. 6 (color online). This snapshot shows the location of the 5% most mobile particles in a system of 4096 particles at a reduced density $\rho = 20$. The mobile particles are represented by cones. The cone base is centered around the initial particle position and the cone orientation gives the direction of displacement. For clarity, the displacements have been multiplied by 2. The figure shows that the most mobile particles are distributed very inhomogeneously over the simulation box.

given time interval. The length of this time interval was chosen equal to the time at which the non-Gaussian behavior peaks. The figure shows that there are large empty spaces in the figure which are occupied by the immobile particles. On average, the displacements of the mobile particles are correlated. The picture shows clearly that clusters of mobile particles span the entire system ($N = 4096$). Much larger systems would be needed to make a systematic study of the shape and distribution of the dynamical heterogeneities.

In summary, structural arrest in an ideal gas is due to the increasing importance of topological constraints. The exponential density dependence of the diffusion coefficient suggests that the particle mobility is facilitated by the spontaneous appearance of “cavities” where the topological constraints on the motion of a particle are temporarily released. As in strong glasses, there is no sharp glass transition. At high densities, the system becomes dynamically heterogeneous and strong non-Gaussian effects in the particle displacements show up. For $\rho \gg 1$, the functions $F_s(q, t/t_\alpha)$ for a given q all collapse onto a single master curve, independent of ρ . A parameter-free theoretical pre-

diction of this observation would be desirable and, in view of the simplicity of the model, probably feasible.

The work of the FOM Institute is part of the research program of FOM and is made possible by financial support from the Netherlands Organization for Scientific Research (NWO) and by EU Contract No. MRTN-CT-2003-504712. C.D. acknowledges financial support by the Engineering and Physical Sciences Research Council (EPSRC). We gratefully acknowledge helpful comments by H.C. Andersen, C.A. Angell, J.-L. Barrat, M.E. Cates, D. Chandler, H.R. Krishnamurthy, H. Löwen, T.V. Ramakrishnan, D.R. Reichman, R. Schilling, F. Sciortino, and T. Voigtmann.

-
- [1] G. Adams and J.H. Gibbs, *J. Chem. Phys.* **43**, 139 (1965).
 - [2] S.F. Edwards and Th. Vilgis, *Phys. Scr.* **T13**, 7 (1986).
 - [3] W. Götze, in *Liquids, Freezing and the Glass Transition*, edited by J.P. Hansen, D. Levesque, and J. Zinn-Justin (North-Holland, Amsterdam, 1991).
 - [4] R. Schilling, in *Collective Dynamics of Nonlinear and Disordered Systems*, edited by G. Radons, W. Just, and P. Häussler (Springer, Berlin, 2004).
 - [5] D. Kivelson, S.A. Kivelson, X.L. Zhao, Z. Nussinov, and G. Tarjus, *Physica (Amsterdam)* **219A**, 27 (1995).
 - [6] J.P. Garrahan and D. Chandler, *Proc. Nat. Acad. Sci. U.S.A.* **100**, 9710 (2003).
 - [7] L. Berthier and J.P. Garrahan, *Phys. Rev. E* **68**, 041201 (2003).
 - [8] E. Zaccarelli *et al.*, *Europhys. Lett.* **55**, 157 (2001).
 - [9] S.S. Ghosh and C. Dasgupta, *Phys. Rev. Lett.* **77**, 1310 (1996).
 - [10] M.E. Cates *et al.*, cond-mat/0310579.
 - [11] D. Frenkel and J.F. Maguire, *Phys. Rev. Lett.* **47**, 1025 (1981); *Mol. Phys.* **49**, 503 (1983).
 - [12] S. Obukohov *et al.*, *J. Phys. I (France)* **7**, 563 (1997).
 - [13] C. Renner, H. Löwen, and J.L. Barrat, *Phys. Rev. E* **52**, 5091 (1995); R. Schilling and G. Szamel, *Europhys Lett.* **61**, 207 (2003); M. Jimenez-Ruiz *et al.*, *J. Phys. Condens. Matter* **14**, 1509 (2002).
 - [14] D.C. Rapaport, *J. Comput. Phys.* **34**, 184 (1980).
 - [15] W. Kob *et al.*, *Phys. Rev. Lett.* **79**, 2827 (1997); C. Donati *et al.*, *Phys. Rev. Lett.* **80**, 2338 (1998); R. Yamamoto and A. Onuki, *Phys. Rev. Lett.* **81**, 4915 (1998).
 - [16] D. Chandler and T. Voigtmann (private communication).
 - [17] In an ideal gas at constant pressure, $\rho \sim 1/T$. Hence the time-density scaling in the present system is similar to the more conventional time-temperature scaling.